Journal of Engineering Mathematics (2005) 51: 351–365
DOI 10.1007/s10665-004-7468-1

On an asymptotic expansion for Carreau fluids in porous media

T. GÖTZ and H.A. PARHUSIP[1]
Department of Mathematics, University of Kaiserslautern, Postbox 3049, D–67653 Kaiserslautern, Germany (goetz@mathematik.uni-kl.de); [1]*Department of Mathematics, Institut Teknologi Bandung, Jl. Ganesha 10, Bandung 40132, Indonesia (hanna_p@dns.math.itb.ac.id)*

Received 28 January 2004; accepted in revised form 8 December 2004

Abstract. Porous-media flow of polymers with Carreau-law viscosities and their application to enhanced oil recovery (EOR) is considered. Applying the homogenization method leads to a nonlinear two-scale problem. In case of a small difference between the Carreau and the Newtonian case an asymptotic expansion based on the small deviation of the viscosity from the Newtonian case is introduced. For uni-directional pressure gradients, which is a reasonable assumption in applications like EOR, auxiliary problems to decouple the micro- from the macrovariables are derived. The microscopic flow field obtained by the proposed approach is compared to the solution of the two-scale problem. Finite-element calculations for isotropic and anisotropic pore-cell geometries are used to validate the accuracy and speed-up of the proposed approach. The order of accuracy has been studied by performing the simulations up to the third-order expansion for the isotropic geometry.

Key words: Carreau law, porous-media flow, two-scale expansion

1. Introduction

Polymer flooding has been found to be an excellent method for improving oil recovery (EOR, Enhanced Oil Recovery). Polymers are added to the injected water to increase its viscosity and to improve the oil-water mobility ratio [1, Chapter 1], [2]. For heavy oil with viscosities 10^3–10^6 times higher than water [3], the water-injection technique as described in [4,5] is not applicable and polymer injection is used. To describe polymer flooding in porous media, engineers use the Darcy filtration law and the porous medium is considered to consist of connected arrays of capillaries [6, Chapter 3], [7,8]. The permeability is either obtained by measurements or deduced from known models such as that of Kozeny-Carman [9].

However, Darcy's law and the permeability can be derived from the microscopic Stokes-flow equations using homogenization techniques, which are asymptotic expansions in the small ratio ε of the microscopic and the macroscopic length scale; see [10, Section 1.4], [11] and references therein. In the Newtonian case, the micro- and macroscale decouple and one obtains a local relation between the pressure gradient and the flow velocity. The homogenization of non-Newtonian flows has been discussed in [12–15]. The resulting filtration laws are in general non-local, *i.e.,* the micro- and macroscale do not decouple. To remedy this drawback in the non-Newtonian case, numerical methods to solve the two-scale homogenized system are used [16,17] or nonlinear filtration laws have been derived; see [18], [19, Chapter 1] and references therein. Non-Newtonian Hele-Shaw flows and their analogies in porous-media equations are also widely discussed in the literature; see [20–22].

The rheologic behavior of polymeric liquids used in EOR is frequently described in the engineering literature by either a power law or the Carreau law [6, Chapter 4]. A recent development of stochastic homogenization for power-law fluids may be found in [23].

Since the concentration of the polymers is rather low, the difference between the real rheologic behavior and the Newtonian case is typically very small. This suggests to introduce a second asymptotic expansion based on the small deviation of the viscosity from the Newtonian case. For uni-directional pressure gradients, which is a reasonable assumption in applications like EOR, we derive auxiliary problems to decouple the micro- from the macrovariables.

According to the power law (sometimes also called Ostwald-de Waele law), the viscosity is given by

$$\eta = \eta(\gamma) = \lambda\, \gamma^{r-2}, \tag{1}$$

where $\gamma = \|\mathrm{D}\boldsymbol{u}\| = \left(\sum_{i,j} (\mathrm{D}_{i,j}\boldsymbol{u})^2\right)^{1/2}$ denotes the shear rate, the rate-of-strain tensor being given by $\mathrm{D}\boldsymbol{u} = \frac{1}{2}\left[\nabla \boldsymbol{u} + \nabla \boldsymbol{u}^{\top}\right]$. The parameters λ and r are called the consistency and the flow index. The flow index r characterizes the fluid: for $r > 2$ the fluid is called dilatant, $r = 2$ corresponds to Newtonian behavior, the range $1 < r < 2$ is called pseudo-plastic and $r = 1$ yields purely plastic flows. We focus in this paper on the pseudo-plastic regime, *i.e.,* $r \in (1, 2)$. Due to its simplicity and ability to fit experimental viscosity data for a large class of fluids, this model is very popular. However, one disadvantage of the power law is that it does not accurately describe the behavior of the viscosity for low shear rates. According to the power law, the viscosity tends to infinity for low shear rates and $r \in (1, 2)$, whereas for real fluids it tends to some constant value η_0 called the zero-shear-rate viscosity. Hence, we consider as a generalization the Carreau law:

$$\eta = \eta(\gamma) = (\eta_0 - \eta_\infty)\left(1 + \lambda\gamma^2\right)^{r/2-1} + \eta_\infty,$$

where $\eta_0 > \eta_\infty > 0,\ \lambda > 0,\ 1 < r < 2$. The parameter λ is a time constant, r is a dimensionless constant describing the slope in the power-law region and η_∞ is the high-shear-rate limit of the viscosity.

Scaling the spatial coordinates with a typical length L and the velocities with a typical velocity U, we obtain the non-dimensional Carreau law of the form

$$\tilde{\eta} = (\tilde{\eta}_0 - \tilde{\eta}_\infty)\left(1 + \tilde{\lambda}\tilde{\gamma}^2\right)^{r/2-1} + \tilde{\eta}_\infty\,, \tag{2}$$

where $\tilde{\eta} = \eta/\eta_R$ is the non-dimensional viscosity, η_R some reference value for the viscosity, $\tilde{\lambda} = (U/L)^2\lambda$ is a dimensionless parameter and $\tilde{\gamma} = (L/U)\gamma$ denotes the non-dimensional shear rate. In the sequel we will always work with this non-dimensional form of the Carreau law and skip the tilde.

Most of the flows involved in polymer processing are slow. Therefore we consider only creeping flow, *i.e.,* low-Reynolds-number flows, neglecting inertial effects.

Although we consider throughout this paper only two-dimensional flows, the proposed method can be generalized to three-dimensional situations. However, the numerical simulations get more involved and require special attention to keep the computational effort within reasonable limits.

This paper is organized as follows. In Section 2 we review the formal homogenization of non-Newtonian flows where the viscosity is modeled by a power or Carreau law. Assuming the porous medium to consist of a periodic arrangement of cells with size ε, we use a two-scale power-series *ansatz* for the velocity and the pressure. If the rheologic parameter λ in the Carreau law is also small, we introduce in Section 3 a second power series with respect to this parameter. This will lead us to a sequence of cell problems similar to the Newtonian case.

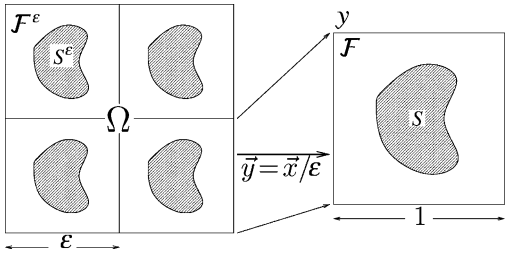

Figure 1. Sketch of the considered geometry. Note that both the macrovariable $\boldsymbol{x}$ and the microvariable $\boldsymbol{y}$ are vectors in $\mathbb{R}^2$.

Section 4 presents numerical simulations to illustrate the accuracy of the proposed asymptotic approach.

Throughout this paper we use boldface italic letters for vectors (*e.g.* $\boldsymbol{u}\in\mathbb{R}^2$) and boldface upright letters for matrices (*e.g.* $\mathbf{D}\in\mathbb{R}^{2\times 2}$).

2. Non-Newtonian porous-media flow

We consider a porous medium $\Omega\subset\mathbb{R}^2$ with a typical dimension $L_{\boldsymbol{x}}$ and call $\boldsymbol{x}\in\Omega$ the macrovariable. We assume that Ω consists of a periodic repetition of an elementary square cell $\mathcal{Y}^\varepsilon$ of size $L_{\boldsymbol{y}}=\varepsilon L_{\boldsymbol{x}}$, where $\varepsilon\ll 1$. This elementary cell contains the fluid part $\mathcal{F}^\varepsilon\subset\mathcal{Y}^\varepsilon$ and the solid part $\mathcal{S}^\varepsilon=\overline{\Omega\backslash\mathcal{F}^\varepsilon}$; see Figure 1.

On the elementary cell we consider the non-dimensional, incompressible Stokes equations given by

$$\varepsilon^2\nabla\cdot[\eta^\varepsilon\,\mathrm{D}\boldsymbol{u}^\varepsilon]=\nabla p^\varepsilon \quad \text{in } \mathcal{F}^\varepsilon, \tag{3a}$$

$$\nabla\cdot\boldsymbol{u}^\varepsilon=0 \quad \text{in } \mathcal{F}^\varepsilon, \tag{3b}$$

$$\boldsymbol{u}^\varepsilon=0 \quad \text{on } \partial\mathcal{S}^\varepsilon. \tag{3c}$$

Analogously to the Newtonian case [10, Section 1.4], we introduce the microvariable $\boldsymbol{y}=\boldsymbol{x}/\varepsilon\in\mathbb{R}^2$ defined on the upscaled elementary cell $\mathcal{Y}$ (with fluid part $\mathcal{F}$ and solid part $\mathcal{S}$) and assume the following two-scale asymptotic expansions for the velocity $\boldsymbol{u}^\varepsilon$ and the pressure p^ε

$$\boldsymbol{u}^\varepsilon(\boldsymbol{x})=\boldsymbol{u}^\varepsilon(\boldsymbol{x},\boldsymbol{y})=\boldsymbol{u}_0(\boldsymbol{x},\boldsymbol{y})+\varepsilon\boldsymbol{u}_1(\boldsymbol{x},\boldsymbol{y})+\varepsilon^2\boldsymbol{u}_2(\boldsymbol{x},\boldsymbol{y})+\cdots,$$
$$p^\varepsilon(\boldsymbol{x})=p^\varepsilon(\boldsymbol{x},\boldsymbol{y})=p_0(\boldsymbol{x},\boldsymbol{y})+\varepsilon p_1(\boldsymbol{x},\boldsymbol{y})+\varepsilon^2 p_2(\boldsymbol{x},\boldsymbol{y})+\cdots,$$

where the coefficient functions $\boldsymbol{u}_i$ and p_i are $\boldsymbol{y}$–periodic. We expand the rate-of-strain tensor $\mathrm{D}\boldsymbol{u}^\varepsilon$ as

$$\mathrm{D}\boldsymbol{u}^\varepsilon(\boldsymbol{x})=\mathrm{D}\boldsymbol{u}^\varepsilon(\boldsymbol{x},\boldsymbol{y})=\varepsilon^{-1}\mathbf{d}_{-1}(\boldsymbol{x},\boldsymbol{y})+\mathbf{d}_0(\boldsymbol{x},\boldsymbol{y})+\varepsilon\mathbf{d}_1(\boldsymbol{x},\boldsymbol{y})+\cdots,$$

where $\mathbf{d}_{-1}=\mathrm{D}_{\boldsymbol{y}}\boldsymbol{u}_0=\frac{1}{2}\left[\nabla_{\boldsymbol{y}}\boldsymbol{u}_0+\nabla_{\boldsymbol{y}}\boldsymbol{u}_0^\top\right]$, $\mathbf{d}_0=\mathrm{D}_{\boldsymbol{x}}\boldsymbol{u}_0+\mathrm{D}_{\boldsymbol{y}}\boldsymbol{u}_1$ and $\mathbf{d}_1=\mathrm{D}_{\boldsymbol{x}}\boldsymbol{u}_1+\mathrm{D}_{\boldsymbol{y}}\boldsymbol{u}_2$.

For a large class of non-Newtonian media, the generalized viscosity η^ε is given as a function of the shear rate $\gamma^2=\|\mathrm{D}\boldsymbol{u}^\varepsilon\|_2^2$. Expanding the shear rate in terms of ε yields

$$\gamma^2=\varepsilon^{-2}\gamma_{-2}+\varepsilon^{-1}\gamma_{-1}+\gamma_0+\cdots,$$

where $\gamma_{-2}=\|\mathbf{d}_{-1}\|_2^2$, $\gamma_{-1}=2\mathrm{tr}\left(\mathbf{d}_{-1}\,\mathbf{d}_0\right)$ and $\gamma_0=\|\mathbf{d}_0\|_2^2+2\mathrm{tr}\left(\mathbf{d}_{-1}\,\mathbf{d}_1\right)$, since all the $\mathbf{d}_i$ are symmetric. Now, the viscosity function $\eta^\varepsilon=\eta(\varepsilon^2\gamma^2)$ can also be written in terms of ε

$$\eta^\varepsilon=\eta_0+\varepsilon\eta_1+\varepsilon^2\eta_2+\cdots,$$

where $\eta_0 = \eta(\gamma_{-2})$, $\eta_1 = \eta'(\gamma_{-2})\gamma_{-1}$ and $\eta_2 = \eta'(\gamma_{-2})\gamma_0 + \eta''(\gamma_{-2})\gamma_{-1}^2/2$.

Plugging the above expansions into (3) and collecting equal powers of ε, we have

$$\nabla_{\boldsymbol{y}} p_0 = 0 \quad \text{for } \boldsymbol{y} \in \mathcal{Y}. \tag{4}$$

Hence $p_0 = p_0(\boldsymbol{x})$, *i.e.,* the leading order p_0 of the pressure is independent of the microvariable $\boldsymbol{y}$. The next-order terms lead to the *two-scale problem*

$$\nabla_{\boldsymbol{y}} \cdot [\eta(\gamma_{-2})\, \mathbf{d}_{-1}] = \nabla_{\boldsymbol{x}} p_0 + \nabla_{\boldsymbol{y}} p_1 \quad \text{in } \Omega \times \mathcal{F}, \tag{5a}$$

$$\nabla_{\boldsymbol{y}} \cdot \boldsymbol{u}_0 = 0 \quad \text{in } \Omega \times \mathcal{F}, \tag{5b}$$

$$\boldsymbol{u}_0 = 0 \quad \text{on } \Omega \times \partial\mathcal{S}, \tag{5c}$$

$$(\boldsymbol{u}_0, p_1) \quad \text{is } \boldsymbol{y}\text{-periodic on } \Omega, \tag{5d}$$

and $\nabla_{\boldsymbol{x}} \cdot \boldsymbol{u}^{\varepsilon} = 0$ as well as the *$\boldsymbol{y}$-periodicity* yield

$$\nabla_{\boldsymbol{x}} \cdot \int_{\mathcal{Y}} \boldsymbol{u}_0 \, \mathrm{d}\boldsymbol{y} = 0 \quad \text{on } \Omega. \tag{5e}$$

In [10, Chapter 3], existence and uniqueness results for problem (5) and Carreau or power-law viscosities are given. Some of the importance of the two-scale asymptotic expansions applied to Newtonian flow in porous media arises from the fact that, for Newtonian fluids, the above two-scale problem (5) separates the macro- and microvariable. Hence, one can derive so-called auxiliary problems that depend solely on the $\boldsymbol{y}$-variable and that can be used to define a permeability tensor.

2.1. Derivation of auxiliary problems

In the Newtonian case, Equation (5a) is linear and reads as $\eta \Delta_{\boldsymbol{y}} \boldsymbol{u}_0 = \nabla_{\boldsymbol{x}} p_0 + \nabla_{\boldsymbol{y}} p_1$. Rewriting $\nabla_{\boldsymbol{x}} p_0$ componentwise, we introduce the *auxiliary problem*

$$\Delta_{\boldsymbol{y}} \boldsymbol{w}_k = \boldsymbol{e}_k + \nabla_{\boldsymbol{y}} \pi_k, \tag{6}$$

where $\boldsymbol{w}_k(\boldsymbol{y})$ and $\pi_k(\boldsymbol{y})$ depend solely on the microvariable. The solution $\boldsymbol{u}_0(\boldsymbol{x}, \boldsymbol{y})$ and $p_1(\boldsymbol{x}, \boldsymbol{y})$ of (5) is then given by

$$\boldsymbol{u}_0(\boldsymbol{x}, \boldsymbol{y}) = \frac{1}{\eta} \sum_k \partial_k p_0(\boldsymbol{x}) \cdot \boldsymbol{w}_k(\boldsymbol{y}),$$

$$p_1(\boldsymbol{x}, \boldsymbol{y}) = \sum_k \partial_k p_0(\boldsymbol{x}) \cdot \pi_k(\boldsymbol{y}).$$

Averaging over the microvariable $\boldsymbol{y}$, we obtain *Darcy's law*

$$\boldsymbol{u}_0(\boldsymbol{x}) = \int_{\mathcal{Y}} \boldsymbol{u}_0(\boldsymbol{x}, \boldsymbol{y}) \, \mathrm{d}\boldsymbol{y} = \frac{1}{\eta} \sum_k \partial_k p_0(\boldsymbol{x}) \int_{\mathcal{Y}} \boldsymbol{w}_k(\boldsymbol{y}) \, \mathrm{d}\boldsymbol{y} =: \frac{\mathbf{M}}{\eta} \cdot \nabla p_0,$$

where $\mathbf{M}$ is the permeability tensor.

To generalize this approach to the non-Newtonian case and to find conditions for the existence of decoupled auxiliary problems, we propose the *ansatz*

$$\boldsymbol{u}_0(\boldsymbol{x}, \boldsymbol{y}) = \sum_k f(\partial_k p_0) \cdot \boldsymbol{w}_k(\boldsymbol{y}), \tag{7a}$$

$$p_1(\boldsymbol{x}, \boldsymbol{y}) = \sum_k g(\partial_k p_0) \cdot \pi_k(\boldsymbol{y}), \tag{7b}$$

where f and g are some yet arbitrary functions. Plugging this *ansatz* for $\boldsymbol{u}_0$ into the shear rate, we obtain

$$\gamma_{-2}(\boldsymbol{x}, \boldsymbol{y}) = \sum_k f(\partial_k p_0)^2 \|\mathrm{D}\boldsymbol{w}_k\|_2^2 + \sum_{k \neq l} f(\partial_k p_0) f(\partial_l p_0) \mathrm{tr}\,(\mathrm{D}\boldsymbol{w}_k \,\mathrm{D}\boldsymbol{w}_l + \mathrm{D}\boldsymbol{w}_l \,\mathrm{D}\boldsymbol{w}_k)\,. \tag{8}$$

and hence the two-scale problem (5a) reads as

$$\sum_k f(\partial_k p_0)\, \nabla_{\boldsymbol{y}} \cdot [(\eta_0(\boldsymbol{x}, \boldsymbol{y})\, \mathrm{D}\boldsymbol{w}_k(\boldsymbol{y})] = \sum_k \partial_k p_0(\boldsymbol{x}) \cdot \boldsymbol{e}_k + \sum_k g(\partial_k p_0) \cdot \nabla_{\boldsymbol{y}} \pi_k(\boldsymbol{y})\,. \tag{9}$$

If the viscosity function separates like $\eta_0(\boldsymbol{x}, \boldsymbol{y}) = \varphi(\boldsymbol{x})\, \psi(\boldsymbol{y})$, we can derive an auxiliary problem similar to (6) depending solely on the microvariable $\boldsymbol{y}$.

Let us restrict ourselves to the case of a uni-directional gradient of the macroscopic pressure, *i.e.,* $\partial_k p_0 = 0$ for all but one k. This assumption is quite realistic in applications like EOR, since the microscopic flow is driven mainly by the pressure difference between the injection point and the well. In this flow regime, the expression for the shear rate (8) simplifies to

$$\gamma_{-2}(\boldsymbol{x}, \boldsymbol{y}) = f(\partial_k p_0(\boldsymbol{x}))^2 \|\mathrm{D}\boldsymbol{w}_k(\boldsymbol{y})\|_2^2 = \tilde{f}(\boldsymbol{x})\, \tilde{\gamma}(\boldsymbol{y})\,. \tag{10}$$

To obtain an auxiliary problem, it is required that

$$\eta(\gamma_{-2}) = \eta\left(\tilde{f}(\boldsymbol{x})\, \tilde{\gamma}(\boldsymbol{y})\right) = \varphi(\boldsymbol{x})\, \psi(\boldsymbol{y})\,. \tag{11}$$

Considering $\partial_{\boldsymbol{y}}\,(\partial_{\boldsymbol{x}}(11)/(11))$ and introducing $z = \tilde{f}(\boldsymbol{x})\, \tilde{\gamma}(\boldsymbol{y})$, we obtain the differential equation

$$\frac{\eta\eta'' - \eta'^2}{\eta^2} z + \frac{\eta'}{\eta} = 0 \qquad \Longrightarrow \qquad (\log \eta)'' z + (\log \eta)' = 0$$

for $\eta = \eta(z)$ with the general solution

$$\eta(z) = c_1 z^n\,.$$

Hence, in the case of a uni-directional macroscopic pressure gradient we can expect auxiliary problems only for Newtonian ($n = 0$) or power-law fluids ($n \neq 0$).

2.2. Power-law fluids

For a power-law fluid, the viscosity is given by (1). Using (10) we obtain $\eta_0 = \lambda\, f(\partial_k p_0(\boldsymbol{x}))^{r-2}\, \|\mathrm{D}\boldsymbol{w}_k(\boldsymbol{y})\|_2^{r-2}$ for the leading term of the viscosity. The two-scale problem (5a) reads

$$\lambda\, f(\partial_k p_0)^{r-1}\, \nabla_{\boldsymbol{y}} \cdot \left(\|\mathrm{D}\boldsymbol{w}_k(\boldsymbol{y})\|_2^{r-1}\, \mathrm{D}\boldsymbol{w}_k(\boldsymbol{y})\right) = \partial_k p_0(\boldsymbol{x}) \cdot \boldsymbol{e}_k + g(\partial_k p_0) \cdot \nabla_{\boldsymbol{y}}\, \pi_k(\boldsymbol{y})\,.$$

Setting $f(\partial_k p_0) = (\partial_k p_0)^{1/(r-1)}$ and $g(\partial_k p_0) = \partial_k p_0$ yields the following auxiliary problem, independent of the macrovariable $\boldsymbol{x}$,

$$\nabla_{\boldsymbol{y}} \cdot \left(\|\mathrm{D}\boldsymbol{w}_k(\boldsymbol{y})\|_2^{r-1}\, \mathrm{D}\boldsymbol{w}_k(\boldsymbol{y})\right) = \boldsymbol{e}_k + \nabla_{\boldsymbol{y}}\, \pi_k(\boldsymbol{y}) \qquad \text{for } \boldsymbol{y} \in \mathcal{F}\,. \tag{12}$$

Once having the solution $\boldsymbol{w}_k(\boldsymbol{y})$, we can compute the zeroth-order approximation of the velocity field

$$\boldsymbol{u}_0(\boldsymbol{x}, \boldsymbol{y}) = (\partial_k p_0(\boldsymbol{x}))^{1/(r-1)}\, \boldsymbol{w}_k(\boldsymbol{y}) \tag{13}$$

and averaging over the microvariable $\boldsymbol{y}$ yields the macroscopic seepage velocity

$$\tilde{\boldsymbol{u}}(\boldsymbol{x}) = (\partial_k p_0(\boldsymbol{x}))^{1/(r-1)} \int_{\mathcal{Y}} \boldsymbol{w}_k(\boldsymbol{y})\, \mathrm{d}\boldsymbol{y}\,. \tag{14}$$

Note, that this derivation is only valid in the case of a uni-directional pressure gradient. Unlike in the Newtonian case, it is not possible to construct the velocity field for arbitrary pressure gradients via superposition.

2.3. Carreau fluids

Using the Carreau model (2) for the viscosity we cannot construct an auxiliary problem, not even in the case of a uni-directional macroscopic pressure gradient. If $\partial_k p_0 = \boldsymbol{a} = \text{const.}$, we can plug (13) into (5a) and obtain the auxiliary problem

$$\nabla_{\boldsymbol{y}} \cdot \left[\eta \left(\|\mathrm{D}\boldsymbol{w}_k(\boldsymbol{y})\|_2^2 \right) \mathrm{D}\boldsymbol{w}_k(\boldsymbol{y}) \right] = \boldsymbol{a} + \nabla_{\boldsymbol{y}} \pi_k(\boldsymbol{y}) \qquad \text{for } \boldsymbol{y} \in \mathcal{F}\,, \tag{15}$$

with

$$\eta \left(\|\mathrm{D}\boldsymbol{w}_k(\boldsymbol{y})\|_2^2 \right) = (\eta_0 - \eta_\infty) \left(\xi_1 + \lambda \|\mathrm{D}\boldsymbol{w}_k(\boldsymbol{y})\|_2^2 \right)^{(r/2-1)} + \xi_2\,, \tag{16}$$

and $\xi_1 = (\partial_k p_0(\boldsymbol{x}))^{1/(r-1)}$, $\xi_2 = \eta_\infty (\partial_k p_0(\boldsymbol{x}))^{-(r-2)/(r-1)}$. Note, that the auxiliary problem (15) is independent of the macroscale. The microscopic velocity $w_k(\boldsymbol{y}) = \boldsymbol{w}_k(\boldsymbol{a}; \boldsymbol{y})$ depends on the pressure gradient $\boldsymbol{a}$, and averaging over the cell, we obtain the macroscopic velocity

$$\tilde{\boldsymbol{u}} = \int_{\mathcal{Y}} \boldsymbol{w}_k(\boldsymbol{a}; \boldsymbol{y})\, \mathrm{d}\boldsymbol{y} = \tilde{\boldsymbol{u}}(\boldsymbol{a})\,. \tag{17}$$

This equation, relating the macroscopic pressure gradient $\boldsymbol{a}$ to the seepage velocity $\boldsymbol{u}$, can be viewed as a nonlinear filtration law, extending Darcy's law from the Newtonian to the non-Newtonian regime.

However, we will not pursue this approach, but rather focus on the rheology parameter λ in the Carreau law. An expansion with respect to this parameter will enable us to derive a sequence of Newtonian two-scale problems for approximating (5). For each of these Newtonian problems we have the auxiliary problem available that separates the macro- and microscale.

3. Asymptotic expansion of the Carreau model

In this section we consider the two-scale problem (5) with a viscosity given by the Carreau law (2). In the case of a small rheology parameter $\lambda \ll 1$, we introduce a second power series for the velocity and pressure with respect to λ. For the sake of simplicity we are satisfied with an expansion up to first-order terms. To obtain the higher-order corrections is a straightforward but tedious algebraic exercise.

The viscosity introducing the nonlinearity in (5a) is given by

$$\eta(\gamma_{-2}) = (\eta_0 - \eta_\infty) \left(1 + \lambda \|\mathbf{d}_{-1}\|_2^2 \right)^{(r/2-1)} + \eta_\infty\,.$$

Expanding with respect to λ up to first order, we obtain

$$\eta \approx \eta^{(0)} + \lambda \eta^{(1)} = \eta_0 + \lambda(\eta_0 - \eta_\infty) \left(\frac{r}{2} - 1 \right) \|\mathbf{d}_{-1}\|_2^2\,. \tag{18}$$

Note, that this power series in λ is an expansion at zero shear rates. This type of expansion is reasonable in EOR, since the viscosity of the polymer-water mixture is only slightly different from the Newtonian viscosity of the water.

Assuming the existence of a power series in λ for $p_0(\boldsymbol{x})$ and the two-scale pressure $p_1(\boldsymbol{x}, \boldsymbol{y})$, we introduce the following *ansatz* for the velocity

$$\boldsymbol{u}_0(\boldsymbol{x}, \boldsymbol{y}) = \boldsymbol{u}_0^{(0)}(\boldsymbol{x}, \boldsymbol{y}) + \lambda \boldsymbol{u}_0^{(1)}(\boldsymbol{x}, \boldsymbol{y}) = \boldsymbol{w}_k^{(0)}(\boldsymbol{y})\, g(\partial_k p_0)^{(0)} + \lambda \boldsymbol{w}_k^{(1)}(\boldsymbol{y})\, g(\partial_k p_0)^{(1)} + \cdots . \tag{19}$$

with $g(\partial_k p_0)^{(0)} = \partial_k p_0$ and $g(\partial_k p_0)^{(1)} = |\partial_k p_0|^2 \partial_k p_0$.

The auxiliary problem at $\mathcal{O}(\lambda^0)$ reads as

$$\begin{aligned}
&\eta_0 \, \Delta_{\boldsymbol{y}} \boldsymbol{w}_k^{(0)}(\boldsymbol{y}) = \nabla_{\boldsymbol{y}} \pi_k^{(0)}(\boldsymbol{y}) - \boldsymbol{e}_k \quad \text{for } \boldsymbol{y} \in \mathcal{F}, \\
&\nabla_{\boldsymbol{y}} \cdot \boldsymbol{w}_k^{(0)}(\boldsymbol{y}) = 0 \quad \text{for } \boldsymbol{y} \in \mathcal{F}, \\
&\boldsymbol{w}_k^{(0)}(\boldsymbol{y}) = 0 \quad \text{for } \boldsymbol{y} \in \partial\mathcal{S}, \\
&\left(\boldsymbol{w}_k^{(0)}, \pi_k^{(0)}\right) \quad \text{is periodic in } \boldsymbol{y}.
\end{aligned} \tag{20}$$

In the next order $\mathcal{O}(\lambda^1)$ the auxiliary problem is given by

$$\begin{aligned}
&\eta_0 \, \Delta_{\boldsymbol{y}} \boldsymbol{w}_k^{(1)}(\boldsymbol{y}) = \nabla_{\boldsymbol{y}} \pi_k^{(1)}(\boldsymbol{y}) - \boldsymbol{e}_k + \boldsymbol{f}(\boldsymbol{w}_k^{(0)}) \quad \text{for } \boldsymbol{y} \in \mathcal{F}, \\
&\nabla_{\boldsymbol{y}} \cdot \boldsymbol{w}_k^{(1)}(\boldsymbol{y}) = 0 \quad \text{for } \boldsymbol{y} \in \mathcal{F}, \\
&\boldsymbol{w}_k^{(1)}(\boldsymbol{y}) = 0 \quad \text{for } \boldsymbol{y} \in \partial\mathcal{S}, \\
&\left(\boldsymbol{w}_k^{(1)}, \pi_k^{(1)}\right) \quad \text{is periodic in } \boldsymbol{y},
\end{aligned} \tag{21}$$

where

$$\boldsymbol{f}(\boldsymbol{w}_k^{(0)}) = -(\eta_0 - \eta_\infty)\left(\frac{r}{2} - 1\right) \nabla_{\boldsymbol{y}} \left(\|\mathrm{D}\boldsymbol{w}_k^{(0)}(\boldsymbol{y})\|^2 \, \mathrm{D}\boldsymbol{w}_k^{(0)}(\boldsymbol{y}) \right). \tag{22}$$

Generally we have to solve for each order $\mathcal{O}(\lambda^j)$ a Newtonian auxiliary problem of the form

$$\begin{aligned}
&\eta_0 \, \Delta_{\boldsymbol{y}} \boldsymbol{w}_k(\boldsymbol{y}) = \nabla_{\boldsymbol{y}} \pi_k + \boldsymbol{f} \quad \text{in } \mathcal{F}, \\
&\nabla_{\boldsymbol{y}} \cdot \boldsymbol{w}_k(\boldsymbol{y}) = 0 \quad \text{in } \mathcal{F}, \\
&\boldsymbol{w}_k(\boldsymbol{y}) = 0 \quad \text{on } \partial\mathcal{S}, \\
&(\boldsymbol{w}_k, \pi_k) \quad \text{is periodic in } \boldsymbol{y}.
\end{aligned} \tag{23}$$

Note that, once having the solution $(\boldsymbol{w}_k^{(j)}, \pi_k^{(j)})$ available, we can advance to the next order $j+1$ and get successively the contributions to compute the velocity $\boldsymbol{u}_0$ according to (19).

4. Simulations

In this section we show some numerical simulations to illustrate the accuracy and speed-up of the asymptotic approach presented in Section 3. We consider a range of parameters that is typical for polymers used in EOR and show two example geometries for the elementary cell representing a simplified "standard" geometry in homogenization theory, as well as a more realistic geometry.

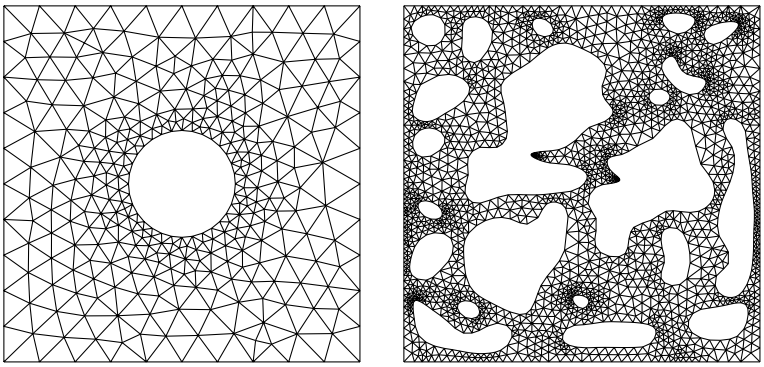

Figure 2. (left): Mesh for the isotropic cell using 580 triangles (denoted as coarse). (right): Mesh for the anisotropic cell using 3672 triangles (denoted as coarse).

Table 1. Parameters of the triangulations used for the isotropic and anisotropic cell geometry.

	Isotropic cell			Anisotropic cell		
	coarse	medium	fine	coarse	medium	fine
NT	580	764	1360	3672	9181	22212
NN	326	424	742	2194	5165	12209

4.1. Geometry and parameters

We consider two different problems, an isotropic and an anisotropic porous medium. In the case of the isotropic medium, the cell $\mathcal{Y}$ is defined as a unit square $[0,1]^2$ with a centered circular inclusion of radius $R = 0{\cdot}15$, see Figure 2(left). For the anisotropic problem we consider the geometry as shown in Figure 2(right) serving as a quite realistic example for natural porous media [24, Chapter 5]. The number of triangles (NT) and nodes (NN) used in the meshes for the isotropic and anisotropic geometry are listed in Table 1.

The parameters used in the simulations are based on the data collected by Hilfer; see [25]. Thus:

- typical pore sizes in oil reservoirs are $L_y \approx 10^{-4}\,\mathrm{m}$;
- microscopic fluid velocities for reservoir flooding are $U \approx 3 \times 10^{-6}\,\mathrm{m\,s^{-1}}$;
- the distance between the injection and production well is about $L_x \approx 100\,\mathrm{m}$.

Hence, the ratio between the microscopic and macroscopic reference length is given by $\varepsilon = L_y/L_x = 10^{-6}$. This small ratio ε serves as the expansion parameter in the homogenization. Concerning the macroscopic pressure p_0, we assume a nonzero pressure gradient in the horizontal $\boldsymbol{e}_1$ direction and a zero pressure gradient in the vertical $\boldsymbol{e}_2$ direction.

For the rheologic properties of the polymer we refer to the measurements for polymers in capillary pipes given in [26], that is,

- density $\rho = 1000\,\mathrm{kg\,m^{-3}}$;
- parameters in the Carreau model: $\eta_\infty = 0{\cdot}001\,\mathrm{Pa\,s}$, $\eta_0 = 0{\cdot}01\,\mathrm{Pa\,s}$, $r = 1{\cdot}3$, $\lambda = 0{\cdot}01\,\mathrm{s}^2$.

These data yield a Reynolds number $\mathrm{Re} = (\rho U L_y)/\eta_0 = 3 \times 10^{-5}$ and a dimensionless rheology parameter $\tilde{\lambda} = \lambda U^2/L_y^2 = 9 \times 10^{-6}$. Since $\tilde{\lambda} \ll 1$, we can use the asymptotic expansion proposed in Section 3.

As already mentioned in the Introduction, for most polymer solutions and polymer melts, the value of r in the Carreau law varies between 1 and 2; see also [6, Chapter 4]. Therefore we consider in our numerical simulations $r = 1{\cdot}3$, $1{\cdot}5$, $1{\cdot}7$ and $1{\cdot}9$. All the numerical simulations are carried out for the dimensionless equations.

4.2. Solution method

The solution of the nonlinear two-scale problem (5) is considered to be exact. To solve this problem we use a Lagrangian method. Here, the idea is to view the incompressibility condition $\nabla_{\boldsymbol{y}} \cdot \boldsymbol{u}_0 = 0$ as a constraint with the pressure p_1 as Lagrangian multiplier. The resulting saddle point problem is discretized by finite elements using quadratic Lagrangian elements for the velocity and linear Lagrangian elements for the pressure. A detailed description of this method applied to nonlinear Stokes problems can be found in [16], [27 Chapter 2], [28, Section 7.5], [29].

In our numerical simulations based on the asymptotic expansion, we first solve the Problems (20) and (21) which are linear Stokes problems and use Equation (19) to obtain the velocity field.

The general outline of the numerical simulation can be summarized in the following steps:

1. Given $\partial_k p(\boldsymbol{x})$, solve Problem (20);
2. Using this solution, compute $\boldsymbol{f}$ by (22) and solve Problem (21);
3. Equation (19) yields the velocity field $\boldsymbol{u}_0(\boldsymbol{x}, \boldsymbol{y})$;
4. Use the solution of (20) as an initial guess to solve the nonlinear Problem (5).

Solving the nonlinear two-scale Stokes problem is rather expensive; hence the asymptotic procedure proposed above might provide a possible speed-up. In Table 2 the speed-up factors of the asymptotic expansion method are listed. Note, that we normalize the execution time of the nonlinear two-scale problem to 1 and that both methods are implemented using FEMLAB® 2.3.

The asymptotic expansion is found to provide a speed-up factor between $1{\cdot}5$ and 2 for the isotropic case and between $1{\cdot}5$ and $3{\cdot}5$ for the anisotropic geometry. One explanation for the rather fast convergence of the nonlinear direct solution might be the fact that the zeroth-order of the asymptotic expansion is used as an initial guess for the nonlinear solver. Hence the direct solution requires only a few iterations, especially in the case of r large, since in this case the viscosity is close to Newtonian.

4.3. Numerical results

4.3.1. *First-order approximation*

We have computed the velocity field inside the isotropic cell using either the full nonlinear Stokes problem (5) (here referred to as *"Exact"*) and the zeroth-order solution according to Problem (20) (*"Newtonian"*) and including the first-order correction (21) (*"Asymptotic"*). The simulations are carried out for the parameter r ranging between $1{\cdot}3$ and $1{\cdot}9$ which covers the region relevant for most polymers.

In order to illustrate the accuracy, we show in Figure 3(left) the relative error between the "exact" solution $\boldsymbol{u}$ and the solution using the asymptotic expansion $\tilde{\boldsymbol{u}}$. The relative error is given by

Table 2. Speed-up factors of the asymptotic expansion compared to the direct solution of the nonlinear two-scale Stokes problem. The execution time of the nonlinear two-scale problem is scaled to 1. In reality it is of the order of 1 minute on the fine mesh of the isotropic cell with $r = 1{\cdot}3$ up to 193 minutes on the fine mesh of the anisotropic cell with $r = 1{\cdot}3$ (1·8 GHz Athlon, 1·5 GB Memory, FEMLAB 2.3). Missing results ('—') indicate, that the direct solution method did not converge

	Isotropic cell			Anisotropic cell		
r	coarse	medium	fine	coarse	medium	fine
1·3	1·95	1·58	1·51	–	–	1·58
1·5	1·52	1·70	1·51	–	1·53	2·30
1·7	1·50	1·35	1·36	3·54	1·52	1·53
1·9	1·52	1·69	1·95	2·88	1·73	3·79

$$E_R(\boldsymbol{y}) = \frac{\|\boldsymbol{u}(\boldsymbol{y}) - \tilde{\boldsymbol{u}}(\boldsymbol{y})\|_2}{\max\limits_{\boldsymbol{y}\in\mathcal{Y}} \|\boldsymbol{u}(\boldsymbol{y})\|_2}. \tag{24}$$

From a practical point of view, using an absolute norm, *e.g.* the error in the flow rate, as suggested by one of the referees, might be more appealing, since it directly shows the implications of the used asymptotics to the predicted productivity of the oil reservoir. However, since we are mainly interested in the applicability of the proposed *ansatz*, we focus on a relative norm based on the primary variables of the problem. In addition to the relative error in the velocity field, Figure 5 provides a comparison of the shear-rates and viscosities in the exact and the asymptotic solutions.

In the case of isotropic media, the maximum of the relative error is about 4·5% and appears on the horizontal cell boundaries, whereas the relative error is smallest close to the surface of the obstacle.

Figure 3(right) shows the horizontal velocity component along the line $y_1 = 0{\cdot}7$, $y_2 \in [0, 1]$ for $r = 1{\cdot}3$. Again, the same behavior as in Figure 3(left) is clearly visible; the error is smallest close to the obstacle (here for $y_2 \approx 0{\cdot}5$) and increases toward the boundaries. A close agreement between the "exact" solution and the asymptotic expansion is found. The solution involving a Newtonian viscosity differs already quite significantly from the "exact" one, indicating the need for the correction terms introduced by the asymptotic expansion.

Analogously to the isotropic case, we consider the complex geometry shown in Figure 2 (right). Again, the simulations are carried out for the parameter r ranging between 1·3 and 1·9 and we compare the "exact" and the asymptotic solution. Due to the complexity of the geometry, the maximal relative errors are larger in the anisotropic case and reach about 10% on the finest triangulation.

In Figure 4(left) the relative error for $r = 1{\cdot}5$ is shown and Figure 4(right) provides a comparison of the velocity profiles analogously to the isotropic geometry.

In Table 3 we list the relative errors for the isotropic and the anisotropic cell for the different triangulations and various values of the parameter r.

For the isotropic geometry the relative errors are independent of the used triangulation, whereas in the anisotropic case the errors depend on the grid. The direct solution of the two-scale problem did only converge on the finest triangulation for the anisotropic geometry case and $r = 1{\cdot}3$. For $r = 1{\cdot}5$ the direct solution converged already on the medium grid. Due to the

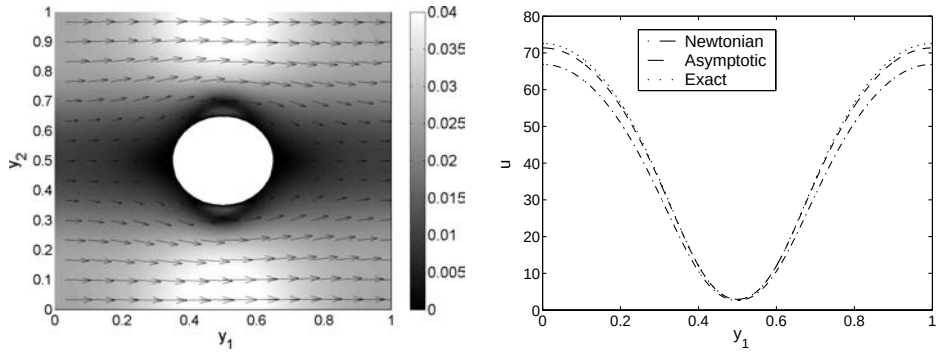

Figure 3. (left): Relative error $E_R(\boldsymbol{y})$ between "exact" solution and asymptotic expansion. The arrows visualize $\boldsymbol{u}(\boldsymbol{y}) - \tilde{\boldsymbol{u}}(\boldsymbol{y})$ and the greyscale shows the magnitude of the relative error. Computed on the fine grid. (right): Velocity profile for $r = 1{\cdot}3$ along the line $y_1 = 0{\cdot}7$, $y_2 \in [0, 1]$. Note that the asymptotic solution('- -') agrees very well the "exact" solution ('. . .').

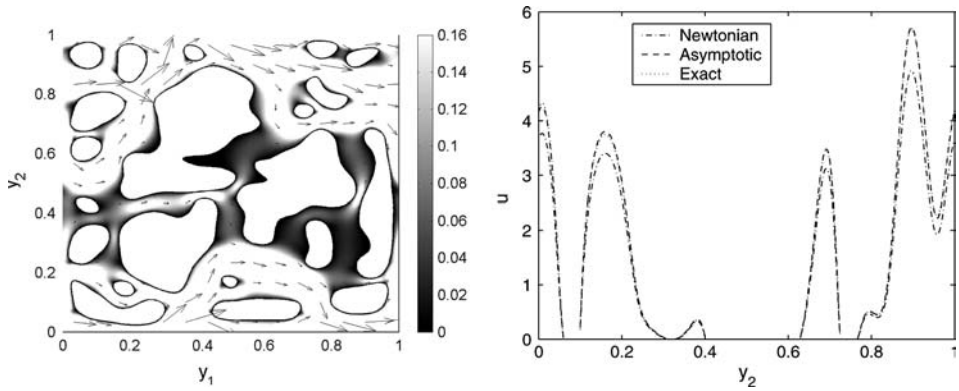

Figure 4. (left): Relative error $E_R(\boldsymbol{y})$ between "exact" solution and asymptotic expansion. The arrows visualize $\boldsymbol{u}(\boldsymbol{y}) - \tilde{\boldsymbol{u}}(\boldsymbol{y})$ and the greyscale shows the magnitude of the relative error. Computed for $r = 1{\cdot}5$ on the medium grid. (right): Velocity profile for $r = 1{\cdot}3$ along the line $y_1 = 0{\cdot}7$, $y_2 \in [0, 1]$ computed on the medium grid. Note, that the asymptotic solution ('–') agrees perfectly with the exact one ('. . .').

Table 3. Maximal relative errors for the two cell geometries, refined triangulations and various values of r. Missing results ('—') indicate, that the direct solution method did not converge.

	Isotropic cell			Anisotropic cell		
r	coarse	medium	fine	coarse	medium	fine
1·3	4·42%	4·44%	4·41%	—	—	8·50%
1·5	2·46%	2·41%	2·36%	—	15·93%	9·96%
1·7	2·28%	2·32%	2·21%	11·66%	9·89%	8·32%
1·9	0·98%	1·01%	0·95%	6·08%	3·99%	3·96%

the nonlinearity in viscosity, small spatial stepsizes are needed in these cases. However, the asymptotic expansion converged on all grids, since it only requires the solution of a linear Stokes equation.

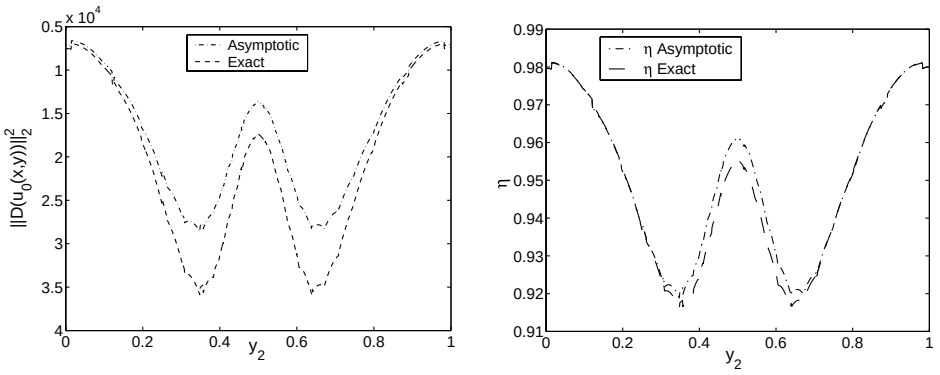

Figure 5. (left): Two scale shear-rate profile for isotropic case computed along the line $y_1 = 0{\cdot}7$, $y_2 \in [0, 1]$ for the isotropic case computed using the zeroth-order cell problem to get $\|D(w_k(y))\|_2^2$ and multiplied by the $(\partial_k p_0)^2$ for the asymptotic profile. (right): Viscosity profile for isotropic case along the line $y_1 = 0{\cdot}7$, $y_2 \in [0, 1]$ computed on the medium grid.

As expected, the errors are largest in the non-Newtonian regime, *i.e.,* for $r = 1{\cdot}3$ and decrease towards the Newtonian regime, *i.e.,* for r increasing for both geometries.

In Figure 5, the shear rates and the resulting nondimensional viscosities are shown the "exact" and the asymptotic solution. For a given dimensionless $\lambda = 9 \times 10^{-6}$ and $r = 1{\cdot}3$ we solve the two-scale and the asymptotic problem on the isotropic geometry. Using (19), the magnitude of the shear rate is given by $\|\mathrm{D}(\boldsymbol{u}_0)\|_2^2 = (\partial_k p_0)^2 \|\mathrm{D}(\boldsymbol{w}_k(\boldsymbol{y}))\|_2^2$. It is clearly visible from Figure 5(left), that the shear-rates are large but still $\lambda \|\mathrm{D}(\boldsymbol{u}_0)\|_2^2$ holds. Figure 5(right) shows the computed viscosities; the viscosity determined by the asymptotic expansion agrees remarkably well with the "exact" viscosity.

4.3.2. *Higher-order approximations*

We have seen in the previous section that the relative errors in the isotropic case are independent of the grids. Hence the relative errors depend solely on the asymptotic expansion with respect to the parameter λ. To analyze the accuracy of the asymptotic method we consider the expansion up to the third order for the isotropic case on the coarse grid. We choose $r = 1{\cdot}3$ because in this regime the nonlinearity is dominant and we vary the values of λ between 9×10^{-9} and 9×10^{-6}.

Figure 6 shows a log-log-plot of the maximum relative error versus the scaled expansion parameter λ. We observe two different regions, where the errors show different behaviors. Note, that the behaviors of errors change around $\lambda = 5{\cdot}4 \times 10^{-7}$, which is found numerically. Hence we choose $\lambda = 5{\cdot}4 \times 10^{-7}$ as a critical value which divides the errors into two regions. The first region covers the parameters $9 \times 10^{-9} \leq \lambda < 5{\cdot}4 \times 10^{-7}$ and the second region is $5{\cdot}4 \times 10^{-7} \leq \lambda < 9 \times 10^{-6}$.

Figure 7 focuses on these two regions. A least-squares method was used to fit a linear function to the data. The slope of this linear fit yields the order of the error. Table 4 lists the obtained orders of the error in the different regions.

In the first region shown in Figure 7 (left), the order of the error is almost equal to 1, independent of the approximation order. Although λ is rather small in this region, the change of the approximation seems not to be caused by a loss of significant figures in the computations. In the second region, see Figure 7 (right) the error behaves almost as expected. For the first-order approximation the error depends nearly linearly on the expansion parameter λ and

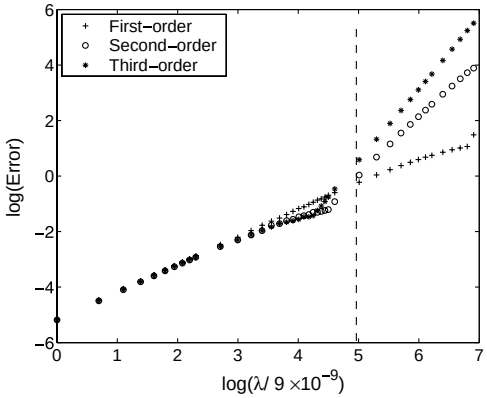

Figure 6. Correlation between the logarithm of $\lambda/9{\cdot}0 \times 10^{-9}$ and the logarithm of the maximum relative error. The vertical dashed line separates the two regions of different error behavior.

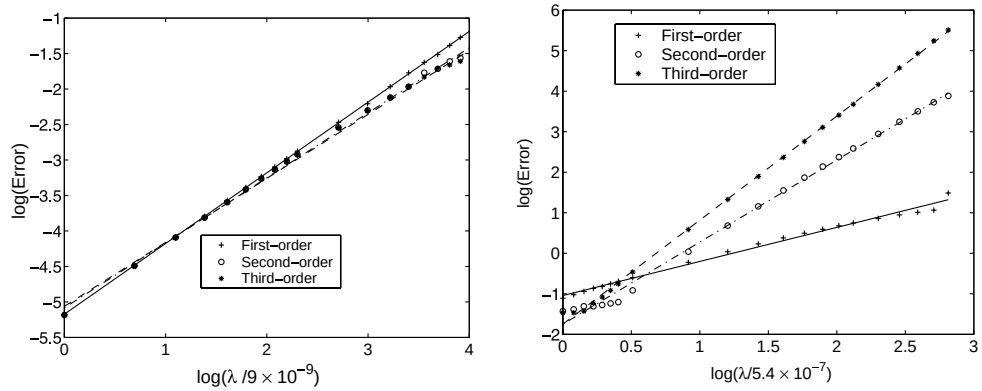

Figure 7. (left): Correlation between the logarithm of $\lambda/9{\cdot}0 \times 10^{-9}$ and the logarithm of the maximum relative error for the region $9{\cdot}0 \times 10^{-9} \leq \lambda < 5{\cdot}40 \times 10^{-7}$. The solid line is the linear fit for the first-order approximation, the dash-dotted line for the second-order and the dashed line for the third-order approximation. (right): Same results as in the left figure for region II $5{\cdot}40 \times 10^{-7} \leq \lambda < 9{\cdot}0 \times 10^{-6}$.

for the second-order expansion it increases quadratically with λ. The deviation for the third-order expansion may be caused by the numerical method.

At the moment we do not have a conclusive explanation for the existence of the two regions with different error behavior. Further investigations into this topic seem to be necessary.

5. Conclusions

Polymer flooding has been found to be an excellent method for improving the output of oil fields, so-called enhanced oil recovery (EOR). Due to the nonlinear rheologic behavior of the added polymers, the flow of these polymers in porous media cannot be modelled using the classical Darcy law. Applying a two-scale expansion to the porous-media equations yields in this situation a coupled two-scale nonlinear system for the velocities and pressures on both the micro- and macroscale. The direct numerical simulation of this system is a non-trivial task, since the coupling of the micro- and macroscale generates a problem in depending on a 4- resp. 6-dimensional space variable in 2d resp. 3d physical space. Hence methods to decouple the micro- from the macroscale are desirable and promise a significant speed-up.

Table 4. Computed orders of the approximation error in the two regions.

	Approximation order		
Region	1	2	3
I	0·99	0·92	0·90
II	0·84	2·02	2·56

The viscosity of the polymer-water solution is modelled using a Carreau-law, where the rheologic parameter λ is typically rather small. Exploiting the smallness of this parameter gives rise to a second asymptotic expansion. In the case of uni-directional pressure gradients we derived auxiliary problems decoupling the micro- and macrovariables. This approach yields a sequence of linear Stokes problems on the micro-scale. Based on the finite-element method, calculations were performed to validate the proposed approach and to compare with the solution of the nonlinear two-scale problem. For different pore geometries and various rheological parameters we found a remarkably good agreement between the asymptotic and the direct solution.

The relative errors introduced by the first-order asymptotic expansion are less than 5% for the isotropic and less than 10% for the anisotropic geometry on a suitable finite-element discretization. The speed-up factor of the asymptotic expansion was found to vary between 1·5 and 35 depending on the used grid, geometry and data. Higher-order expansions were studied in the isotropic case for various values of λ with $r = 1{\cdot}3$.

Acknowledgements

The research of H. A. Parhusip was partly supported by a grant from the DAAD (German Academic Exchange Service, (code *A/00/41574*)) and partly by a grant from The Abdus Salam ICTP, Trieste (code *STEP-02/01*). The authors also want to thank the referees for their useful comments and valuable suggestions.

References

1. K.S. Sorbie and D. Phil, *Polymer Improved Oil Recovery*. Glasgow: Blakie (1991) 359pp.
2. A. Bartelds, *The Influence of Inaccessible and Excluded Pore Volume on Polymer Flooding*. PhD thesis, Delft University of Technology (1998) 205 pp.
3. M. London, IRIS explorer in oil recovery, *Visualization Development Environments Proceedings* 2000. http://flow.arc.ab.ca/london/vde 2000/paper.pdf
4. T.W. Patzek and D.B. Silin, Water injection into a low-permeability rock – 1: hydrofracture growth. *Trans. Porous Media* 43 (2001) 537–555.
5. G.Q. Tang and A. Firoozabadi, Effect of pressure gradient and initial water saturation on water injection in water-wet and mixed-wet fractured porous media. *SPE Reserv. Eval. Engng.* (2001) 516–524.
6. R.B. Bird, R.C. Armstrong and O. Hassager, *Dynamics of Polymeric Liquids, (Vol. 1).* New York: Wiley (1977) 649pp.
7. K.S. Sorbie, P.J. Clifford and E.R.W. Jones, The rheology of pseudoplastic fluids in porous media using network modeling. *J. Colloid Interface Sci.* 130 (1989) 510–534.
8. K.S. Sorbie and Y. Huang, Rheological and transport effects in the flow of low concentration xanthan solution through porous media. *J. Colloid Interface Sci.* 145 (1991) 75–87.

9. A. Koponen, M. Kataja and J. Timonen, Simulations of single-fluid flow in porous media. *Int. J. Modern Phys. C* 9 (1997) 1505–1521.
10. U. Hornung, *Homogenization and Porous Media*. New York: Springer (1997) 279 pp.
11. A.Y. Beliaev and S.M. Kozlov, Darcy equation for random porous media. *Comm. Pure Appl. Math* 49 (1996) 1–34.
12. A. Mikelic and I. Aganovic, Homogenization of stationary flow of miscible fluids in a domain with a grained boundary. *SIAM J. Math. Anal.* 19 (1988) 287–294.
13. G. Allaire, Homogenization of the Stokes flow in a connected porous medium. *Asympt. Anal.* 2 (1989) 203–222.
14. A. Bourgeat and A. Mikelic, Homogenization of a polymer flow through a porous medium. *Nonlin. Anal., Theory, Methods Appl.* 26 (1996) 1221–1253.
15. A. Mikelic, Homogenization theory and applications to filtration through porous media. In: A. Fasano (ed.), *Filtration in Porous Media and Industrial Application* (2000) pp. 127–214.
16. O. Gipouloux and Z. Abdel-Malek, Computation of the filtration laws through porous media for a non-Newtonian fluid obeying the power law. *Comput. Geosci.* 1 (1997) 127–153.
17. B. Bang and D. Lukkasen, Application of homogenization theory related to Stokes flow in porous media. *Appl. Math.* 44 (1999) 309–319.
18. E. Marusic-Paloka and A. Mikelic, The derivation of a nonlinear filtration law including the inertia effects via homogenization. *Nonlin. Anal., Theory Methods Appl.* 42A (2000) 97–137.
19. G.I. Barenblatt, V.M. Entov and V.M. Ryzhik, *Theory of Fluid Flows Through Natural Rocks.* Dordrecht: Kluwer (1990) 395 pp.
20. H. Begehr, R.P. Gilbert, Non-Newtonian Hele-Shaw flows in $n \geq 2$ dimensions. *Nonlin. Anal., Theory Methods Appl.* 11 (1987) 17–47.
21. L. Kondic, P. Palffy-Muhoray and M.J. Shelley, Models of non-Newtonian Hele-Shaw flow. *Phys. Rev. E* 54, No. 5 (1996) 4536–4539.
22. R.P. Gilbert and M. Fang, Nonlinear systems arising from nonisothermal, non-Newtonian Hele-Shaw flows in the presence of body forces and sources. *Math. Comput. Model.* 35 (2002) 1425–1444.
23. A. Fadili, P.M.J. Tardy and J.R.A. Pearson, A 3D filtration law for power-law fluids in heterogeneous porous media. *J. Non-Newtonian Fluid Mech.* 106 (2002) 121–146.
24. M. Griebel, T. Dornseifer and T. Neunhoeffer, *Numerical Simulation in Fluid Dynamics*. Philadelphia: SIAM (1998) 217 pp.
25. R. Hilfer, Transport and relaxation phenomena in porous media. *Adv. Chem. Phys* 92 (1996) 299–424.
26. H.P.S. Siregar, *Characterisation Rheologique des Solutions Aqueuses de Polyacrylamide Utilisees en Recuperation Assistee du Petrole*. Ph.D. thesis, University of Bordeaux, France (1980) 103 pp.
27. R. Glowinski, J.L. Lions and R. Tremolieres, *Numerical Analysis of Variational Inequalities*. Amsterdam: North Holland (1981) 776 pp.
28. R. Glowinski, *Numerical Methods for Nonlinear Variational Problems*. New York: Springer (1984) 493 pp.
29. V. Sarin, *Efficient Iterative Methods for Saddle Point Problems*. Ph.D. thesis, University of Illinois at Urbana-Champaign (1997) 76 pp.